



**HAL**  
open science

# Modelling Log-End Cracks Due to Growth Stresses: Calculation of the Elastic Energy Release Rate

Delphine Jullien, Aziz Laghdir, Joseph Gril

► **To cite this version:**

Delphine Jullien, Aziz Laghdir, Joseph Gril. Modelling Log-End Cracks Due to Growth Stresses: Calculation of the Elastic Energy Release Rate. *Holzforschung*, 2003, 57 (4), 10.1515/HF.2003.060 . hal-01946583

**HAL Id: hal-01946583**

**<https://hal.science/hal-01946583>**

Submitted on 6 Dec 2018

**HAL** is a multi-disciplinary open access archive for the deposit and dissemination of scientific research documents, whether they are published or not. The documents may come from teaching and research institutions in France or abroad, or from public or private research centers.

L'archive ouverte pluridisciplinaire **HAL**, est destinée au dépôt et à la diffusion de documents scientifiques de niveau recherche, publiés ou non, émanant des établissements d'enseignement et de recherche français ou étrangers, des laboratoires publics ou privés.

# Modelling Log-End Cracks Due to Growth Stresses: Calculation of the Elastic Energy Release Rate

By Delphine Jullien<sup>1</sup>, Aziz Laghdir<sup>2</sup> and Joseph Gril<sup>1</sup>

<sup>1</sup>Laboratoire de Mécanique et Génie Civil, Université Montpellier 2, Montpellier, France

<sup>2</sup>Département des Sciences du bois et de la forêt, Université Laval, Québec, Canada

## Keywords

Growth stress  
Green wood  
Eucalyptus  
Fracture mechanics  
Finite elements method

## Summary

The occurrence of log-end cracks, due to the release of growth stress pre-existing in the standing tree, causes severe damage at the early stage of wood transformation. A mechanical model based on Griffith's theory for elastic-fragile materials has been developed to explain the observed patterns: a crack can only progress when the elastic energy release rate ( $G$ ) exceeds the toughness ( $G_c$ ) of the material for the given fracture mode and orientation. At each stage of the crack propagation,  $G$  was calculated using the finite-element method. The influence of various parameters related to the rigidity components, the initial growth stress field or the crack geometry has been investigated, based on a set of experimental data gathered on a population of Eucalyptus. In all cases the high  $G$  values just after crack initiation are followed by a marked decrease until the periphery has been reached. Their order of magnitude for a typical log is similar to  $G_c$  values measured independently on similar material, thus supporting the validity of the approach.

## Introduction

Log-end cracks consecutive to tree felling and cross-cutting are a clear demonstration of the existence of residual stresses in living stems. These so called growth stresses result from cell-wall maturation: after new cells have been produced in the cambium and achieved their primary expansion, they undergo a reinforcement stage with the formation of a secondary wall, ending with a maturation process characterised by lignification, transverse swelling and, usually, axial shrinkage of the newly formed wood (Archer 1986). Cross-cutting can be analysed as the creation of a free surface in a pre-stressed volume; the consecutive stress redistribution is equivalent to the axial pulling of the heart and pressure of the periphery, which favours the heart splitting of the log ends. Subsequent sawing induces further transformation defects like board deformation or further splitting along the pith. These phenomena, more considerable in hardwoods and in the case of tension wood occurrence, have been extensively reviewed (Kübler 1987), along with useful considerations about their viscoelastic nature and hygrothermal activation. This author and others (Wilhelmy and Kübler 1973; Byrnes and Archer 1977) have already produced finite-element calculations of the displacement field associated with cross-cutting, which are close in their principle to the technique used in the present work.

From a practical viewpoint, log-end cracks are of particular interest. Together with basic geometrical features

like log diameter and curvature or pith eccentricity, they can be easily visualised in the field or in an industrial context. In the case of fast-growing hardwood species like Eucalyptus, saw millers try to minimise the growth-stress related losses by empirically taking into account the visible crack pattern during log manipulation. From the viewpoint of solid mechanics, crack propagation under the action of a mechanical stress can be analysed using energetic concepts derived from Griffith theory (Bui 1978). Our work aims to test how well such mechanical analyses can explain the observed patterns of log-end cracks. In the present paper, a method of numerical analysis will be proposed.

For the sake of clarity we will refer here to a specific case where a number of consistent observations have been made, which will serve for the numerical application. The question raised here is whether mechanical engineers are able to explain some of the observed features of log-end cracking by using the available information on mechanical properties.

## Theory and Numerical Method

### Energetic approach

The analysis of crack propagation used here is based on the 2nd law of thermodynamics, leading to the incremental expression:

$$G_c dA + dW < 0 \text{ or } -dW/dA > G_c \quad (1)$$

where  $dW$  is the variation in elastic energy stored in the body

when the crack area extends by  $dA$ , and  $G_c$  is the energy consumed per creation of a unit area of crack. The contribution of dynamic terms has been neglected, and no external load is acting on the volume. According to Griffith theory, the toughness  $G_c$  is an intrinsic property of the material, and can be determined experimentally for any orientation of crack surface (and fracture mode). The quasi-fragile behaviour of wood loaded transversally to the fibres justify the application of this theory originally designed for crack propagation in glass, and the observed dominance of an opening mode (mode I) makes it possible to neglect the contribution from other fracture modes. Equation (1) can be also written:

$$G > G_c \quad (2)$$

where  $G = -dW/dA$  is the "elastic energy release rate".  $G$ , in contrast to  $G_c$ , depends on the geometry and behaviour of the whole structure, as well as on its formation and loading history, because the initial stress distribution in the log depends strongly on the way the successive wood rings were deposited. The evaluation of  $G$ , therefore, requires a calculation based on a mechanical model.

#### Computation of energy release

A linear relationship is assumed between the stress  $\sigma$  and the small strain  $\varepsilon$ :  $\varepsilon = S\sigma$ , where  $\varepsilon$  and  $\sigma$  are second-order tensors and  $S$  is a tensor of order 4 named compliance. The linearity of this expression allows the use of the initial state of the log just before felling ( $\sigma^i$ ) as reference:

$$\Delta\varepsilon = S\Delta\sigma \quad (3)$$

where  $\Delta\varepsilon$  is the strain relative to the state before felling, and  $\Delta\sigma$  the corresponding stress increase. After propagation of a crack up to a given level of free surface (A), a condition of zero force has to be written for all points of (A):

$$0 = \sigma \cdot n = (\sigma^i + \Delta\sigma) \cdot n \quad \text{or} \quad \Delta\sigma \cdot n = -\sigma^i \cdot n \quad (4)$$

where  $n$  is a unit vector perpendicular to the surface (A), which includes the free surface created by cross-cutting the log. Thus, the existence of the free surface has the same effect as applying a force opposed to that existing in the standing tree. Adding to (3) and (4) conditions of static equilibrium and kinematic compatibility, we end up with a well-formulated mechanical problem having a single solution  $\Delta\sigma$  and associated strain  $\Delta\varepsilon$ . The energy required for the calculation of  $G$  can be obtained as the elastic energy by integration over the whole volume  $V$ :

$$W = \frac{1}{2} \int (\sigma + \Delta\sigma) \cdot S(\sigma + \Delta\sigma) dV \quad (5)$$

Assuming an initial stress field locked in a standing tree, we can calculate the corresponding amount of elastic energy stored in a log cross-cut off this tree. Assuming that a given heart crack appears in the pith of this same log, we can calculate the amount of elastic energy released by the existence of this new surface.

In the following, R, T, L indicate the radial, tangential and longitudinal directions, respectively. We use engineering notations for the stress, strain and compliance tensors, with Young's moduli  $E_R = 1/S_{11}$ ,  $E_T = 1/S_{22}$ ,  $E_L = 1/S_{33}$ , shear moduli  $G_{TL} = 1/S_{44}$ ,  $G_{RL} = 1/S_{55}$ ,  $G_{RT} = 1/S_{66}$ , Poisson's ratios  $\nu_{TL}$ ,  $\nu_{LT}$ ,  $\nu_{RL}$ ,  $\nu_{LR}$ ,  $\nu_{RT}$ ,  $\nu_{TR}$ , linked to each other through:  $\nu_{RT}/E_R = \nu_{TR}/E_T = -1/S_{12}$ ,  $\nu_{RL}/E_R = \nu_{LR}/E_L = -1/S_{13}$ ,  $\nu_{TL}/E_T = \nu_{LT}/E_L = -1/S_{23}$ .

## Experimental Data Required for the Model

### Materials and methods

A population of 177 interspecific hybrid Eucalyptus (*E. urophylla* x *E. grandis*) aged 3 to 7 years from plantations in Congo was used. Complementary information has been also obtained from a few Eucalyptus trees from the Gharb region in Morocco, about 30 years old (7 *E. Camaldulensis*, 7 *E. grandis*, 2 *E. gomphocephala*). On all standing trees, the surface growth stress has been evaluated at breast height and at 8 regular positions around stem periphery using the single-hole method (Fournier *et al.* 1994). The relative displacement of two pins in  $\mu\text{m}$ , termed "growth stress indicator" (GSI), must be roughly multiplied by  $12 \times 10^{-6}$  to produce an estimate of the locked-in longitudinal growth strain, which in turn can be multiplied by  $E_L$  to yield the longitudinal growth stress. On the Congo trees, the length and orientation of log-end cracks were measured one month after felling and cross-cutting. From the Congo trees, 7 were selected so as to represent contrasting combinations of high/low GSI/crack intensity. On these the material properties were obtained from diametral boards cut as near as possible to the level of GSI measurements. Toughness was measured in green state according to the Gustafsson method, described in Schatz (1995), and corresponds to a rupture in mode I of the radial plane (RL) in the radial direction (R). Elastic constants were also measured in green state: rods of dimension 200 mm (L) x 36 mm (R) x 36 mm (T) were cut at 1 to 3 radial positions, each cut into 6 specimens  $20 \times 20 \times 30 \text{ mm}^3$  oriented in the 3 orthotropic directions (R, T, L) and the 3 diagonal directions in the RT, RL and TL planes. The specimens were extracted from each rod so as to have their central parts well aligned in the fibre direction; an additional specimen served to measure the basic density ( $D_b$ , oven-dry weight divided by green volume). They were compressed along their height so as to remain in the elastic range, and the strain in the central part was recorded, using MTS equipment. The slope of the load-displacement curve yielded elastic moduli  $E_L$ ,  $E_R$ ,  $E_T$ ,  $E_{RT}$ ,  $E_{RL}$  and  $E_{TL}$ . The moduli in the diagonal directions involve shear moduli and Poisson's ratios, e.g.,  $1/E_{RL} = [(1-\nu_{RL})/E_R + (1-\nu_{LR})/E_L + 1/G_{RL}]/4$ . On the other hand, radial variations of density ( $d$ ) and longitudinal Young's modulus ( $E_L$ ) were measured on radial series of rods 360 mm (L) x 20 mm (R) x 20 mm (T), using a free-free vibration method (Bordonné 1989). Some Morocco trees were used to measure more sets of elastic constants, while on others the internal pattern of the cracks was studied using a staining method (Jullien *et al.* 2000).

### Constitution of a set of consistent data

The experimental results are thoroughly analysed in Laghdir (2000). Here only the main conclusions will be given, in view of the use for the numerical model.

### Geometry

To represent a typical case of our population, the simulated log will be assumed to be cylindrical, with radius  $R=0.1$  m and height  $2h=1.4$  m, and containing a central pith of radius  $R_0=0.002$  m. The crack shape shown in Figure 1 is suggested from the observations on the Morocco trees (Jullien *et al.* 2000): it is quasi-triangular with a depth  $H$  at the pith level and a radial length  $L$  on the log end. When the periphery has been reached ( $L=R$ ), a lateral opening  $D$  appears. The crack propagates through a vertical translation, with a constant shape ratio ( $k$ ):

$$k = (L-R_0)/H \quad \text{for } L < R ; \quad k = (R-R_0)/(H-D) \quad \text{for } L = R$$

Only the upper half of the log ( $0 < z < h$ ) will be simulated, assuming a symmetrical behaviour of the log.

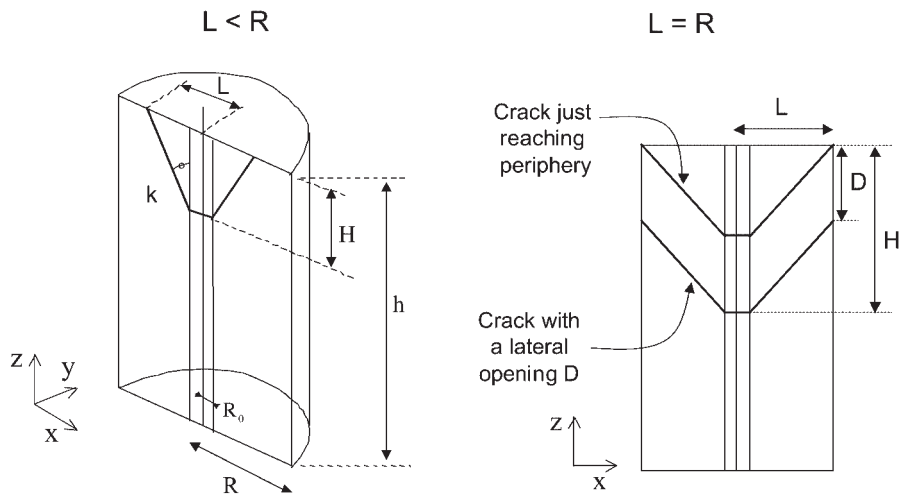


**Fig. 1.** Crack shape and geometrical parameters.

**Table 1.** Material properties used for the simulations

Rigidity components (MPa)	Basic density (g/cm <sup>3</sup> )
$E_L = (27.3 D_b - 1.15) \times 10^3$	$D_b = 0.15 \rho + 0.4$ with $\rho = r/R$ , relative distance to pith ( $0 < \rho < 1$ )
$E_T = 1.625 \times 10^3 D_b - 165$	
$E_R = 0.5 E_T + 630$	<b>Poisson's ratios</b> $\nu_{RT} = 0.75$ $\nu_{LR} = 0.30$ $\nu_{LT} = 0.45$
$G_{RL} = 1.5 E_T + 825$	
$G_{TL} = 0.5 E_T + 980$	
$G_{RL} = 0.8 E_T + 80$	

**Table 2.** Parameters of the initial stress field

Asymmetric part	Symmetric part
$p_2 = 12.5$ MPa	$q = -0.75$ MPa
$n_2 = 1$	$p_1 = 12.5$ MPa
$m = 2$	$n = 1$
$\Delta\theta = 30^\circ$	$n_1 = 1$
$\theta_0 = 90^\circ$	

Constitutive equations

Although a positive correlation between the growth stress level and Young's modulus ( $E_L$ ) has been observed on similar material (Baillères 1994), no clear relation could be made evident in the population investigated; therefore the influence of tension wood on the rigidity will not be accounted for in the simulations.  $E_L$  has been observed to vary linearly with  $D_b$ , which itself varies linearly with the radius  $r$  (distance to the pith). A significant correlation between  $D_b$  and the tangential Young's modulus  $E_T$  has also been observed. Finally, more or less significant correlations have been obtained between  $E_T$  and the other rigidity components. Poisson's ratios were needed to evaluate the shear moduli; values for green beech estimated after measurements by Launay *et al.* (1984) were used. These observations led us to propose a model of behaviour based on the basic density  $D_b$ , with an intermediary variable  $E_T$ , as given in Table 1.

Initial growth stress

The inner distribution of initial growth stress in the standing tree was not measured, so it had to be given a reasonable shape to feed the numerical model. It will be assumed independent of the axial coordinate  $z$ . Transverse components will be supposed axisymmetric and given as a function of the relative distance to pith  $\rho = r/R$  by:

$$\sigma_R^i(\rho) = q[\rho^n - 1]/n ; \sigma_T^i(r) = q[(1+n)\rho^n - 1]/n$$

where  $q$  is the surface stress in the T direction, and  $n$  a constant. In the L direction an asymmetric term will be added:

$$\sigma_L^i(\rho) = p_1 f(\rho; n_1) + p_2 f(\rho; n_2) g[\theta; m]$$

with

$$f(\rho; n) = (2+n)\rho^n/n - 2/n ; g(\theta; m) = 2 \frac{|\theta - \theta_0|^m}{|\Delta\theta|^m}$$

where  $\theta$  is the angular position in the cylindrical system,  $\theta_0$  the peak direction,  $2\Delta\theta$  the peak width,  $m$  a shape factor of the peak,  $p_1$  the level of the axisymmetric part,  $p_2$  that of the additional asymmetric part,  $n_1, n_2$  and  $m$  factors characterising the shape of the radial profiles and circumferential distributions. This expression was designed to fit at the periphery with experimental observations of residual strains in hardwoods (Fournier *et al.* 1994; Sassus 1998), while maintaining self-equilibrium for each angular sector and ensuring the same limit  $-2(p_1/n_1 + p_2/n_2)$  for all angles when  $r \rightarrow 0$ . A standard set of parameters are presented in Table 2:  $p_1, p_2, m, \Delta\theta, \theta_0$  characterising the peripheral distribution of longitudinal growth stress, were fitted to represent typical values for the Congo population; the choice for  $n_1$  and  $n_2$  is partly justified by previous work by Gérard (1994) showing that the observed deflections of quarter-sawn of Eucalyptus is mostly compatible with an assumed linear radial variation of the longitudinal growth stress.

Log-end crack patterns

On the 177 Congo trees, patterns of 2, 3 or 4 cracks were observed, in the respective proportions of 22%, 67% and 11%,

often of different lengths and separated by an angle varying from 45 to 180°. In 26% of the logs at least one crack had reached the periphery, although this was less frequent in the case of double cracks. The following simulations being based on sets of material properties measured on the same population; they ought to be able to predict, to some degree at least, the observed features of log-end cracking.

### Results of Numerical Simulations and Discussion

Calculations are conducted using a finite element package (Modulef), allowing a step-by-step spatial discretisation.

#### *Influence of geometrical parameters*

To observe the sensitivity of calculations to different parameters, we consider the standard case described previously and use as reference two mechanical states of the log: (i) after the cross-cutting operation, and (ii) after appearance of a double crack just reaching the periphery with no lateral opening ( $L=R$  and  $D=0$ ), shape ratio  $k=2$  and orientation perpendicular to the growth stress peak (Fig. 2). In both cases, we investigate the influence of parameters on the amount of energy release.

The elements constituting the mesh are hexahedral. Their number is governed by the number of elements along the radius  $N_R$  and the number of elements around the periphery  $N_T$ . The number of elements along the height of the log depends on these two parameters and on the length of the log. Figures 3 and 4 show the evolution of the energy release in the two considered cases, function of  $N_R$  when  $N_T=16$ , and function of  $N_T$  when  $N_R=10$ : these two values appear to be a good compromise between computer time and precision of calculations, with energy amounts seeming to be well stabilised. In Figures 5 and 6 we investigate the influence of the pith radius  $R_0$ . In the two cases, the energy release becomes stable for low values of the pith radius: a pith radius of 2% seems to be correct for our purpose. Another way to look at the influence of the pith consists in running calculations where the pith has been replaced by a cylindrical hole of the same radius: for low values of the pith radius (less than 2%), the amount of energy release is not much affected by the absence of pith. We will use this new geometry in some further calculations.

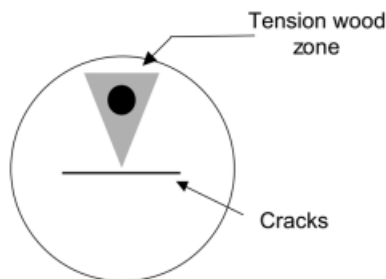


**Fig. 2.** Position of the tension wood zone relative to the crack direction in the standard case.

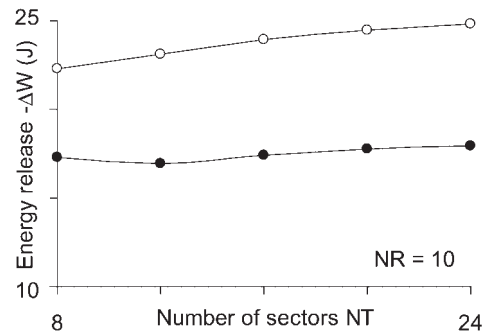


**Fig. 3.** Evolution of the energy release, after cross-cutting (●) and after a crack reaching the periphery (○), for 10 subdivisions along the radius, function of the element size in the tangential direction.

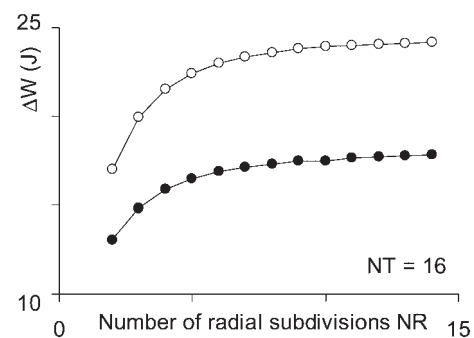


**Fig. 4.** Evolution of the energy release, after cross-cutting (●) and after a crack reaching the periphery (○), for 16 subdivisions around the circumference, function of the number of elements in the radial direction.

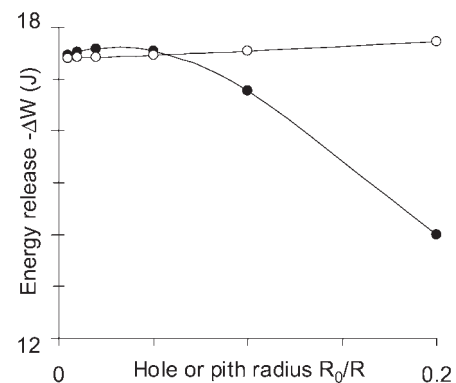


**Fig. 5.** Evolution of the energy release after cross-cutting, function of the hole (●) or pith (○) radius.

#### *Propagation criteria: the reference case*

Considering the cross-cut log, we can investigate the appearance and the propagation of cracks. To calculate the rate  $G$  in Equation (2), the total energy  $W$  can be replaced by  $\Delta W$ , the difference between the energy after crack and after cross-cutting. The toughness  $G_c$  will be

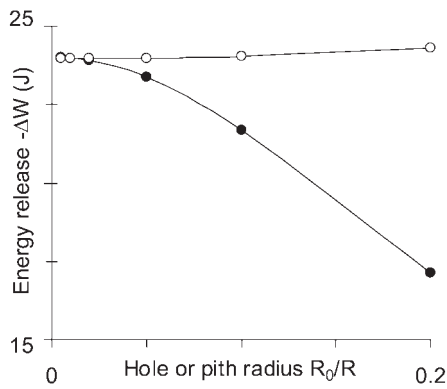


**Fig. 6.** Evolution of the energy release after a crack reaching the periphery, function of the hole ● or pith ○ radius.

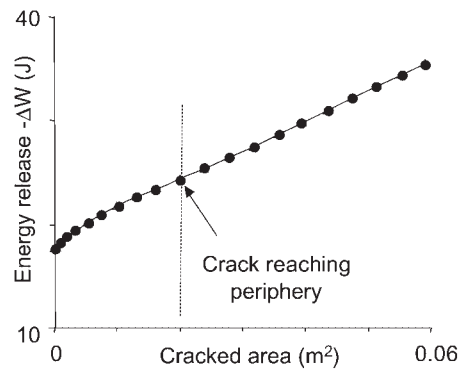


**Fig. 7.** Evolution of the energy release during the propagation of a standard crack (crack with 2 branches).

assumed constant over the log. Figures 7 and 8 show, respectively, the evolution of the energy release ( $-\Delta W$ ) and the rate  $G$ , during the propagation of a double crack, as functions of the cracked area. Not surprisingly, the energy release increases with crack surface. However, the rate curve evidences three critical steps: (1) at the beginning, the elastic energy release rate is very high, about  $700 \text{ J/m}^2$ , which can be explained by the initiation of the crack following the cross-cutting; (2) then the rate decreases sharply to  $250 \text{ J/m}^2$ , corresponding to the crack reaching the periphery; (3) finally, it increases and becomes stable at the fairly low level of about  $300 \text{ J/m}^2$ .

Now, let us compare 3 possible values of the assumed constant toughness  $G_c$ . If  $G_c = G_{c1} = 750 \text{ J/m}^2$ , the propagation criterion is never satisfied, so the existence of a local defect, even big, would not induce any crack propagation. If  $G_c = G_{c2} = 300 \text{ J/m}^2$ , the criterion may be satisfied: if a small crack previously exists at the pith, it will propagate to the level corresponding to the intersection point between the curve and the straight line of equation  $y = G_{c2}$ , which means in this case two opposite cracks of length about the half of the radius. Finally, if  $G_c = G_{c3} = 200 \text{ J/m}^2$ , the propagation criterion is satisfied as soon as a small defect existed previously; in this case, the crack would propagate along the whole log.

This reference case evidences steps of propagation: relatively easy appearance of a small heart crack; difficult propagation to the periphery; easy propagation of the lateral opening along the log as soon as the crack has reached the periphery. The values of  $G$  calculated for the standard case were based on the average behaviour of the population used for the study. They range from  $750 \text{ J/m}^2$  at crack initiation to  $250 \text{ J/m}^2$  at the periphery, compared to the rate  $G_c$  values measured on the same Eucalyptus population, typically  $250 \pm 50 \text{ J/m}^2$ . In the second case described above, the propagation can hardly lead to a crack reaching the periphery. This is consistent with the experimental observation on those logs that exhibited double cracks. This prediction, however, is only valid for the pattern of two cracks that has been simulated. Since it is not dominant for Eucalyptus, we will have to consider also other crack patterns.

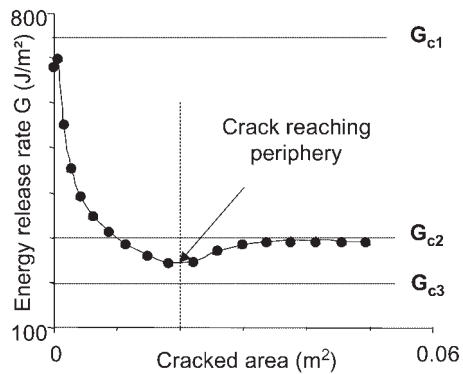


**Fig. 8.** Evolution of the energy release rate during the propagation of a standard crack (crack with 2 branches).

*Influence of mechanical parameters*

The following calculations have been also made using the standard case of a double crack perpendicular to the growth stress peak, but now have been conducted for different lengths of cracks ( $0 < L < R$ ) and also for cracks with lateral openings ( $0 < D < 2R$ ). In all following graphs, the stage where the periphery has been reached by the cracks is indicated.

**Rigidity components**

First, we study the sensitivity of the energy release to the 9 components  $S_{ij}$  of the compliance. From the reference case, we calculate the new energy release when each of the components  $S_{ij}$  has been reduced by 10% (corresponding to an increase 10% of the elastic modulus), all the others parameters being fixed. Figure 9 gives, for each component, the variation in the energy release as a function of the cracked surface. Generally, the energy release is much more sensitive in the case of cross-cutting than in the further steps of crack propagation. The reduction of most compliance components leads to an augmentation of energy release, except for  $S_{12}$  and  $S_{66}$ , which have the opposite effect. It is especially sensitive to the longitudinal rigidity  $E_L = 1/S_{33}$ , with about 5% de-

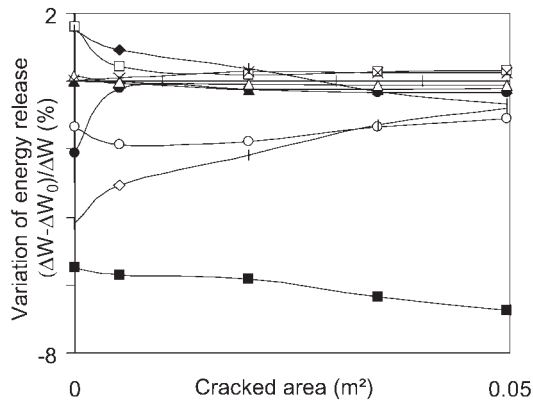


**Fig. 9.** Influence of rigidity components  $S_{11}$ —●—  $S_{22}$ —○—  $S_{33}$ —■—  $S_{12}$ —□—  $S_{23}$ —▲—  $S_{13}$ —△—  $S_{44}$ —◆—  $S_{55}$ —◇—  $S_{66}$ —×— on the elastic energy release.

crease for cross-cutting and 7% for cracks with a high lateral opening. It is also quite sensitive to the tangential rigidity  $E_T=1/S_{22}$ , with a diminution of about 1 to 2% for cross-cutting or for cracks. Sensitivity to shear rigidity  $G_{RL}=1/S_{55}$  is given by a good 4% for cross-cutting, but this effect becomes lower when the crack propagates. For  $S_{12}$  and  $S_{11}$  also, the effect is only marked at the cross-cutting stage, it vanishes in the propagation, whereas for  $S_{13}$ ,  $S_{23}$  and  $S_{66}$  the effect is always small. The influence of  $G_{TL}=1/S_{44}$  is peculiar: 2% increase at the beginning, less when the crack propagates, and a slight increase, of less than 1%, when the crack has reached the periphery. This sensitivity study evidences the importance of some components such as  $E_L$ ,  $E_T$ ,  $G_{RL}$  and  $G_{TL}$ ; it is also useful for estimating the error on the energy calculation due to the error on the experimental evaluation of compliance or rigidity components. These calculations have been conducted considering fixed growth stresses, calculations based on fixed residual strains would lead to somewhat different results.

#### Rigidity gradient

In the reference case, the basic density  $D_b$  varies from 0.4 at the pith to 0.55 g/cm<sup>3</sup> at the periphery, corresponding to a rigidity variation of 10 to 14 GPa for  $E_L$ , and 0.5 to 0.7 for  $E_T$ . It is compared in Figure 10 to two other cases where the average properties remain unchanged: (i) a constant  $D_b$  of 0.5 g/cm<sup>3</sup>, leading to  $E_L=12.5$  GPa and  $E_T=0.65$  GPa; (ii) a pronounced gradient with a variation of  $D_b$  from 0.3 to 0.6 g/cm<sup>3</sup>, leading to  $E_L$  from 7 to 15 GPa and  $E_T$  from 0.3 to 0.8 GPa. In the 3 cases, the energy release follows the same evolution. Homogeneous rigidity leads to less energy release and a higher gradient to more. The higher gradient case presents a higher maximum rate  $G$  at the beginning and a lower minimum value when cracks just reach the periphery. In other words, the rigidity gradient helps to create the

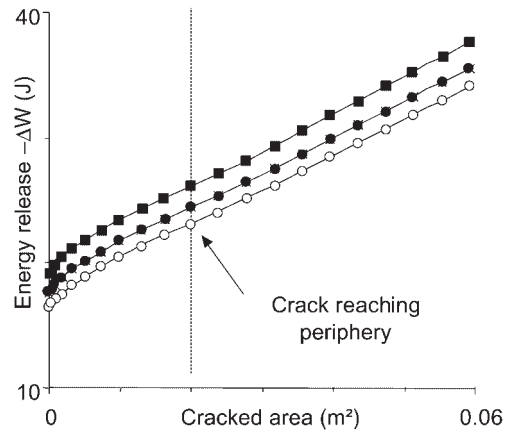


**Fig. 10.** Evolution of the energy release during the propagation of a 2-branch crack for 3 gradients of rigidity from the pith to the periphery: ●  $D_b$ : 0.4–0.55 ○  $D_b$ : 0.5 ■  $D_b$ : 0.3–0.6.

small initial crack, but prevents it from quickly reaching the periphery. In the final step, corresponding to the lateral opening,  $G$  does not seem to depend much on the rigidity gradient.

#### Initial growth stress

In all preceding simulations, the initial distribution of residual stresses was maintained unchanged with a double crack perpendicular to the tension wood zone and a given level of peripheral growth stress. Taking for the rigidities the reference value given in Table 1, we compare now five cases: (1) reference ( $p_1=p_2=12.5$  MPa,  $q=-0.75$  MPa); (2) marked tension wood occurrence with higher longitudinal stress ( $p_2=37.5$  MPa); (3) no tension wood, leading to axisymmetric stress ( $p_2=0$ ); (4) stronger transverse growth stress ( $q=-1.5$  MPa); (5) no transverse growth stress ( $q=0$ ). In each case, all other parameters have reference value as in Table 2. Figure 11 shows similar tendencies in all cases, but with varying levels. The parameter  $p_2$ , linked to the intensity of longitudinal stress in the tension wood zone, has a huge influence on the amount of energy release. The effect of  $q$  variation is weaker, especially at the latest stage: this result seems to indicate that radial and tangential residual stresses have some influence at the early stages of propagation. After the periphery has been reached, the “bending” allowed by the running crack involves essentially the redistribution of the longitudinal component of the stress.

#### Crack pattern

##### Influence of crack number

Let us now compare different cases of crack propagation, with regard to the number of cracks and the position of the tension wood zone relative to the cracks. The 6 studied cases are presented in Figure 12: the first num-

ber indicates the number of cracks, and the second the orientation of the tension wood zone relative to the cracks. In all crack patterns, the energy release during the propagation follows the same evolution mode. The 2-crack mode releases more energy than the 3 and 4 cracks at the beginning, but less in the later stages. Figure 13 shows that, particularly for cracks reaching periphery, the rate  $G$  is higher in the 3- and 4-crack modes; both exhibit similar trends but with a slight preference for the 3-crack mode. The influence of the position of cracks relative to the tension wood zone is very weak at the beginning and becomes stronger at periphery: for 2 cracks, compared to  $2/90^\circ$  (reference case), in  $2/0^\circ$  mode  $G$  is slightly higher at the heart, but decreases and reaches lower values at the periphery. The higher values for cracks with large lateral openings can be intuitively explained by the bending of the two parts of the log: in

the  $2/90^\circ$  mode, the cracks go through the tension wood zone, and thus allow the release of most initial stresses during the bending of the two parts. The influence of the tension wood zone orientation, however, is lower in the 3- and 4-crack modes. We can note, however, a small preference (higher  $G$ ) for  $3/60^\circ$  and  $4/45^\circ$ , where the cracks avoid the tension wood zone, compared to their respective counterparts  $3/0^\circ$  and  $4/0^\circ$ . Finally, the 2-crack mode is privileged for small cracks, but following propagation, 3- and 4-crack modes become more efficient with a weak preference for the 3-crack mode in the last steps of propagation. All these results are consistent with the statistical distribution of cracking mode observed in the sample population, mentioned in the introduction, with a prevalence of the 3-crack mode and a general trend for the main crack to avoid the tension wood zone.

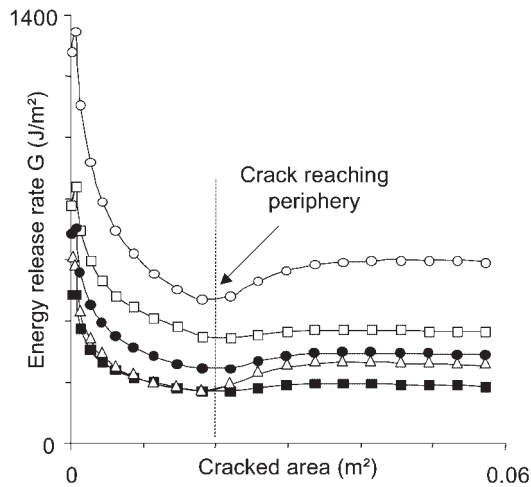


**Fig. 11.** Influence of initial residual stress field on the energy release rate:  $\bullet$  standard case  $P_1 = 12.5$  Mpa,  $P_2 = 12.5$  Mpa,  $q = -0.75$  MPa,  $\circ$   $P_2 = 37.5$  MPa,  $\blacksquare$   $P_2 = 0$ ,  $\square$   $q = -1.5$  MPa,  $\blacktriangle$   $q = 0$ .

**Influence of the crack shape**

Until now, all the calculations considered a crack slope (ratio of depths to radial extension) of 2. In Figure 14 the three slope values of 1, 2 and 3 have been compared. Here calculations have been conducted for the  $3/60^\circ$

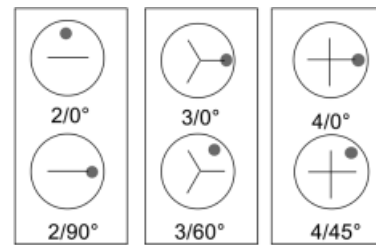


**Fig. 12.** Different cases of crack propagation, with regard to the number of cracks and the position of the tension wood zone relative to the cracks: the first number indicates the number of cracks, and the second the orientation of the tension wood zone relative to the cracks.

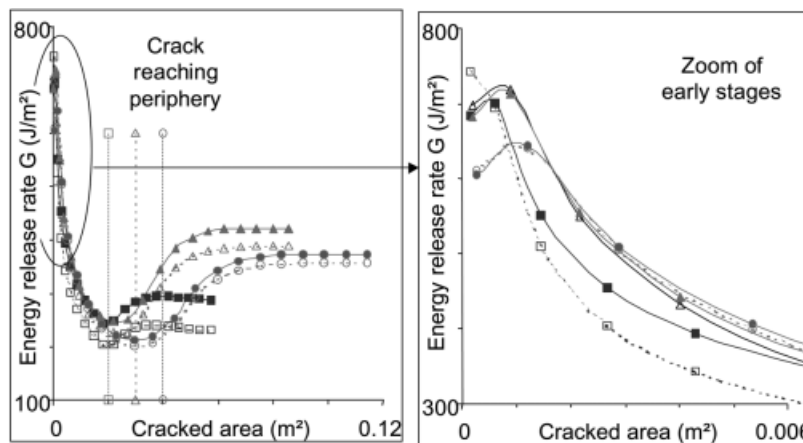


**Fig. 13.** Elastic energy release rate for the 6 cases of crack propagation shown in Figure 12:  $\square$   $2/0^\circ$   $\blacksquare$   $2/90^\circ$   $\triangle$   $3/0^\circ$   $\blacktriangle$   $3/60^\circ$   $\circ$   $4/0^\circ$   $\bullet$   $4/45^\circ$ .

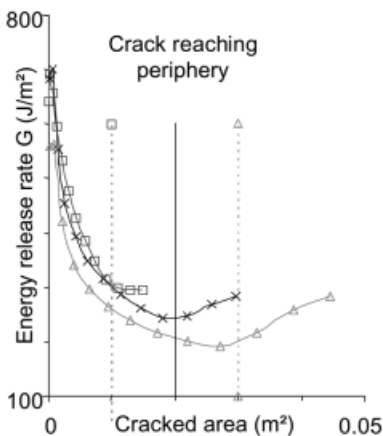


Fig. 14. Influence of the crack slope:  $\square$ -1  $\times$ -2  $\triangle$ -3.

mode. At the beginning, the  $G$  is higher for slopes 1 and 2. But later on, a preference appears for slope 1. Slope 2 always releases more energy than slope 3. This analysis suggests that the propagation of heart cracks does not necessarily occur at constant slope, and leads to the perspective of a modelling taking into account a possible variation of slope and more complex shapes of cracks.

### Conclusions

The propagation of heart cracks due to growth stress release could be interpreted by a classical mechanistic formulation. Applying Griffith theory, the possibility of the propagation is expressed by the elastic energy release rate ( $G$ ) exceeding the intrinsic toughness of the wood material in the observed direction and mode of propagation ( $G_c$ ). The order of magnitude of  $G$  calculated by the finite-elements method, using typical experimental values gathered on a population of Eucalyptus, was consistent with the value of  $G_c$  measured independently for the same material.

To demonstrate the capacity of the numerical tool to account for the various situations encountered in practice, a number of cases of cracking patterns and propagation have been simulated. A fully convincing validation of the software would require an exhaustive set of experimental data obtained on carefully matched material, which was not completely available. However, the results obtained so far are very encouraging because the conclusions gained from the simulation reflected correctly the observed trends in the studied population. The considerable impact of the existence of a tension wood zone, for instance, is correctly predicted, as well as the preference for the 3-crack mode.

In the present work, the cracking pattern has been oversimplified, as compared to reality where branches of different length and depth are generally observed. In a coming version, the pattern will be allowed more freedom, so as to make the evolution of crack orientation and extent one of the outputs of the calculation.

### Acknowledgements

The experimental data used for the simulations were obtained in collaboration with Henri Baillères from CIRAD-Forêt (Biotech project) and Abdelrahim Famiri from Centre National de la Recherche Forestière, Rabat, Morocco (PRAD nb.97-12).

### References

- Archer, R.R. 1986. Growth Stresses and Strains in Trees. Springer Series in Wood Science. Ed. E. Timell. Springer Verlag, Berlin.
- Baillères, H. 1994. Précontraintes de croissance et propriétés mécanophysiques de clones d'Eucalyptus (Pointe Noire – Congo): Hétérogénéités, corrélations et interprétations histologiques. PhD, University Bordeaux 1, France.
- Bordonné, P.A. 1989. Module dynamique et frottement intérieur dans le bois: Mesures sur poutres flottantes en vibrations naturelles. PhD, Institut National Polytechnique de Lorraine, Nancy, France.
- Bui, H.D. 1978. Mécanique de la Rupture Fragile. Masson, Paris.
- Byrnes, F.E. and R.R. Archer. 1977. Calculation of residual strains in log ends due to cross cutting. *Wood Sci.* 10, 81–84.
- Fournier, M., B. Chanson, B. Thibaut and D. Guitard. 1994. Mesure des déformations résiduelles de croissance à la surface des arbres: Observation sur différentes espèces. *Ann. Sci. For.* 51, 249–258.
- Gérard, J. 1994. Contraintes de croissance et valorisation du bois des Eucalyptus de plantation au Congo. PhD, University Bordeaux 1, Bordeaux, France.
- Jullien, D., A. Famiri, J. Gril and A. Laghdir. 2000. Observation of log-end cracks caused by growth stress in Eucalyptus. *In: 3rd Plant Biomechanics Conference, Badenweiler (Freiburg), Germany.* Thieme-Verlag, Stuttgart. pp. 483–486.
- Kübler, H. 1987. Growth stresses in trees and related wood properties. *For. Prod. Abstracts.* 10, 61–119.
- Laghdir, A. 2000. Modélisation de la fissuration en bout de grumes liée aux contraintes de croissance. Application aux Eucalyptus. PhD dissertation. University Montpellier 2, Montpellier, France.
- Launay, J., M. Mudry and F. Giletta 1984. Etude expérimentale de l'influence du taux d'humidité sur l'élasticité du bois. Colloque du Groupe Français de Rhéologie, Paris.
- Sassus, F. 1998. Déformations de maturation et propriétés du bois de tension chez le hêtre et le peuplier: mesures et modèles. PhD, Ecole Nationale du Génie Rural, des Eaux et des Forêts. Montpellier, France.
- Schatz, T. 1995. Zur Bestimmung der Bruchenergie rate GF bei Holz. *Holz Roh- Werkst.* 53, 171–176.
- Wilhelmy, V. and H. Kübler. 1973. Stresses and checks in log ends from relieved growth stresses. *Wood Sci.* 6, 136–142.

Received April 9<sup>th</sup> 2002

D. Jullien  
J. Gril  
Laboratoire de Mécanique et Génie Civil  
Université Montpellier 2  
CC81, Pl. E. Bataillon  
34095 Montpellier  
France

A. Laghdir  
Département des Sciences du bois et de la forêt  
Université Laval  
Québec, G1K 7P4  
Canada